INVESTIGATION ON THE POTENTIAL OF ALOS-2 SINGLE LOOK COMPLEX DATA FOR MASSIVE LANDSLIDE DETECTION

Pinglan GE [1], Hideomi GOKON [2], Kimiro MEGURO [3] and Shunichi KOSHIMURA [4]

ABSTRACT: The 2018 Hokkaido Eastern Iburi Earthquake, occurred on September 6, triggered numerous landslides, disrupting transportation, communication, as well as electricity and power service. A rapid mapping of the massive earthquake-induced landslides was important for directing emergence response efforts. This study investigated the potential of synthetic aperture radar (SAR) images, which could be obtained even in harsh weather, for massive landslide detection. Applied data were ALOS-2 single look complex (SLC) images acquired before and after the earthquake, from which, both intensity and phase information can be derived. First, potential parameters, including the intensity difference, correlation coefficient, and normalized coherence difference, were selected and calculated. Then visual interpretation was carried out to analyze and compare their capabilities for landslide detection by overlaying ground truth data to the calculated parameter images. Results indicate that all the three parameters show some different characteristics in earthquake-induced landslide areas. Whereas the intensity difference image displays clear lower and higher values, the correlation coefficient and normalized coherence difference images show lower values in the landslide areas. In addition, it seems that the landslide direction can be speculated roughly from the intensity difference image, owing to the decreased and increased pixel values caused by the wiping away and piling up of hillside stuffs. Further study will focus on the relation construction between the actual landslides and the potential image characteristics.

Key Words: landslide, synthetic aperture radar (SAR), single look complex (SLC), intensity difference, correlation coefficient, normalized coherence difference

INTRODUCTION

There is a high probability that landslides will be triggered when earthquake occurred in mountainous areas. Earthquake-induced landslides are considered to be responsible for more deaths globally than any other secondary hazard caused by earthquakes (Marano et. al., 2010). They can cause damages to transportation, communication, electricity and power, isolating remote communities and interfering emergency relief work (Cui et. al., 2009). Therefore, a rapid mapping of landslide distribution following a disaster is important for directing

[1] Ph.D. Student, Graduate School of Engineering, The University of Tokyo
[2] Assistant Professor, Institute of Industrial Science, The University of Tokyo
[3] Professor, Institute of Industrial Science, The University of Tokyo
[4] Professor, International Research Institute of Disaster Science, Tohoku University

rescue efforts and limiting resource allocation delays.

Remote sensing data, such as optical images and synthetic aperture radar data (SAR), can be valuable data sources for rapid landslide mapping, due to their large cover, quick response, and no contact capabilities. Optical data are easily to be interpreted since they provide images as human eyes view the earth. However, they highly rely on sunlight for imaging, and hence are unable to be obtained in bad weather and at night. SAR images, conversely, are relatively difficult for interpretation, but are available in any weather conditions owing to the active characteristics of radar sensors. Therefore, SAR data may provide a solution to the rapid landslide mapping even in harsh weather.

Actually, SAR data have already been widely used for landslide slow-moving activity monitoring through various techniques, such as differential interferometry SAR (InSAR) (Strozzi et. al., 2005), persistent scatter interferometry (Confuorto et. al., 2017; Zhao et. al., 2018), and offset tracking (Mulas et. al., 2016). However, studies on their capabilities of mapping landslides are still limited to individual landslides or catchments with limited accuracy (Xue et.al., 2018; Konishi and Suga, 2018; Burrows et. al., 2019). This study aims to provide a comprehensive investigation on the potential of SAR single look complex (SLC) data for massive landslide detection, and compare as well as select favorable potential features for further relation construction between actual landslides and image characteristics. Valuable parameters that can be derived from the SLC images and have the potential to extract landslide areas were first selected and calculated. Visual interpretation was then carried out to analyze and compare their capabilities for landslide area extraction.

RESEARCH AREA AND DATASET

On September 6 at 3:08 am (Japan Standard Time), a powerful earthquake measuring a moment magnitude of 6.6 Mw struck the Iburi area in southern Hokkaido, Japan. This earthquake, officially known as Hokkaido Eastern Iburi Earthquake, occurred at 42.686°N, 141.929°E with a depth of 35 km and claimed 41 lives (USGS). It severely disrupted the electrical service, transportation and communication in Hokkaido area, leaving 5.3 million residents without power and causing a damage of over 367.5 billion yen (Mainichi Shimbun, 2018). According to Yamaguchi and Yamazaki (2018), this intense earthquake triggered more than 6000 landslides over 20×20 km area near Atsuma Town, due to the extremely moist soil caused by the powerful typhoon Jebi occurred just several days before the earthquake. Most landslides were shallow and several meters deep-seated, with some wiping away houses at the foot of slopes. Among all the 41 casualties in the earthquake, 36 people were killed by landslides.

The Japanese Advanced Land Observing Satellite-2 (ALOS-2) captured the affected areas before and after the earthquake in the Level 1.1 format at August 9, 2018, August 23, 2018, and September 6, 2018, respectively. Level 1.1 of the ALOS-2 satellite data is defined as range and single look azimuth compressed data represent by complex I and Q channels to preserve the magnitude and phase information. It means the product is SLC data that can be used for interferometry processing (JAXA, 2014). The two pre-event and one post-event images covered an area of 55km×70km from left looking ascending track with an off-nadir angle of 37.8 degree. The acquisition mode of the images was stripmap ultra-fine mode single polarization (UBS), with a spatial resolution

of 3m and a polarization mode of horizontal transmit/horizontal receive (HH). A summary of these data is shown in **Table 1**.

Table 1. The description of the ALOS-2/PALSAR-2 data in the study

Data (yyyy/mm/dd)	Data Type	Data Format	Data Level	Mode	Polarization	Spatial Resolution	Orbit Direction	Off-nadir Angle
2018/08/09	ALOS-2/ PALSAR-2	CEOS	L1.1 (SLC)	UBS	HH	3m	Left Looking/ Ascending	37.8 °
2018/08/23	ALOS-2/ PALSAR-2	CEOS	L1.1 (SLC)	UBS	HH	3m	Left Looking/ Ascending	37.8 °
2018/09/06 (13:37)	ALOS-2/ PALSAR-2	CEOS	L1.1 (SLC)	UBS	HH	3m	Left Looking/ Ascending	37.8 °

ALOS-2: The Advanced Land Observing Satellite-2; PALSAR-2: The Phased Array type L-band Synthetic Aperture Radar-2; CEOS: Committee on Earth Observation Satellites; SLC: Single Look Complex; UBS: Ultra-fine mode Single polarization; HH: Horizontal transmit/Horizontal receive.

METHODOLOGY

Principle and parameter selection

As introduced in the **RESEARCH AREA AND DATASET** section, the obtained data are Level 1.1 SLC single polarization products, in which both magnitude and phase information were preserved. Therefore, all features that can be derived from the SAR intensity and phase information, and have the ability to measure ground changes can be potential parameters for the exploration of landslide mapping in this case.

Intensity means the backscattering received by a SAR sensor after sending microwaves to ground targets. It not only depends on radar system parameters (e.g. frequency, polarization and incidence angles), but also relates to ground target characteristics (e.g. roughness and moisture content). Therefore, usually, the intensity information changes in SAR images can indicate target changes in actual ground surface, and seems to have the capacity of providing valuable information for landslide mapping. Commonly used intensity parameters for ground change detection include the intensity difference and correlation coefficient. The intensity difference can be simply calculated by subtracting the pre-event intensity image using the post-event intensity image as shown in Eq.1. Regions with large absolute values of the difference represent large ground changes, and vise verse.

$$d = Ib - Ia \tag{1}$$

where d is the intensity difference, and Ib and Ia are pixel intensity values in post-event and pre-event SAR images.

The correlation coefficient of intensity between two images can be calculated according to Eq.2. Its values range from -1 to 1, and can also be used for ground change measurement, with a low value representing large ground changes, and a 1 value meaning no ground changes.

$$r = \frac{N\sum_{i=1}^{N} Ia_i Ib_i - \sum_{i=1}^{N} Ia_i \sum_{i=1}^{N} Ib_i}{\sqrt{\left(N\sum_{i=1}^{N} Ia_i^2 - \left(\sum_{i=1}^{N} Ia_i\right)^2\right)\cdot\left(N\sum_{i=1}^{N} Ib_i^2 - \left(\sum_{i=1}^{N} Ib_i\right)^2\right)}} \quad (2)$$

where r is the correlation coefficient, N is the total number of pixels within a certain window, i is the sample number, and Ia and Ib are pixel intensity values in the pre-event and post-event SAR images.

Phase is a property of periodic phenomenon, referring to the starting point or advancement (fraction) of a wave relative to an arbitrary initial value (ESA, 2014). It depends on the distance between the satellite sensor and the ground target since the path length of a signal to ground and back usually contain a number of whole wavelength plus some fraction of a wavelength. Phase difference is sensitive to ground changes, and can be applied through SAR interferometry technique for deformation monitoring and detection (Massonnet and Feigl, 1998; Zhao et al., 2012), or digital elevation model (DEM) generation (Lanari et al., 1996; Neelmeijer et al., 2017). It contains range information that is accurate to a small fraction of the radar wavelength, and therefore is able to detect and measure tiny path length differences with centimetric or even millimetric accuracy (Moreira et al., 2013). Coherence is a by-product of SAR interferometry, which means the cross-correlation of phase information in two images (Eq.3) and can be used to judge whether a good interferogram can be formed in advance. The values of coherence range from 0 to 1, and can also be used to measure ground changes, with a low value indicating large ground changes between the two timings of radar acquisition.

$$\gamma = \frac{E\langle c_1 c_2^* \rangle}{E\langle c_1 c_1^* \rangle E\langle c_2 c_2^* \rangle} \quad (3)$$

where γ is the coherence, c_1 and c_2 are the corresponding complex pixel values of two acquisition dates, c^* means the complex conjugate of c, and E means the expected value.

To sum up, all of the intensity-related difference and correlation coefficient, as well as the phase-related difference (i.e. interferogram) and coherence have the capability to measure ground changes, and are considered as potential candidates for massive landslide detection in this case.

Image calculation

To calculate the intensity-related and phase-related potential parameters mentioned above, Sentinel Application Platform (SNAP) and ArcGIS software were applied to process the two pre-event and one post-event SAR SLC images. SNAP is an open source common architecture jointly developed by Brockmann Consult, Array Systems Computing and C-S for earth observation data exploitation. In this study, it was mainly used to perform interferometry processing and extract basic intensity and phase information from the complex images. ArcGIS is a geographic information system for working with maps and geographic information. It was mainly applied for the calculation of relevant parameters for instance the intensity correlation coefficient.

To obtain the intensity images for the calculation of intensity difference and correlation coefficient, calibrating, speckle reduction, terrain correction and coregistration were executed sequentially according to Veci

(2016). To obtain the pre- and co-event interferogram and coherence images, interferometry process was carried out in SNAP step by step, which includes the coregistration of pair images, interferogram formation and coherence estimation, topographic phase remove, goldstein phase filtering, and terrain correction.

The calculated pre- and post-event intensity images are shown in **Figure 1**. And the computed pre- and co-seismic coherence images are shown in **Figure 2**. Interferograms were not shown there because fringes in the calculated co-seismic interferogram are not visible, and therefore cannot provide valuable information for landslide identification in this case. It is said that the interference failure was due to the 35km earthquake depth beneath the surface (Karimzadeh and Matsuoka, 2018).

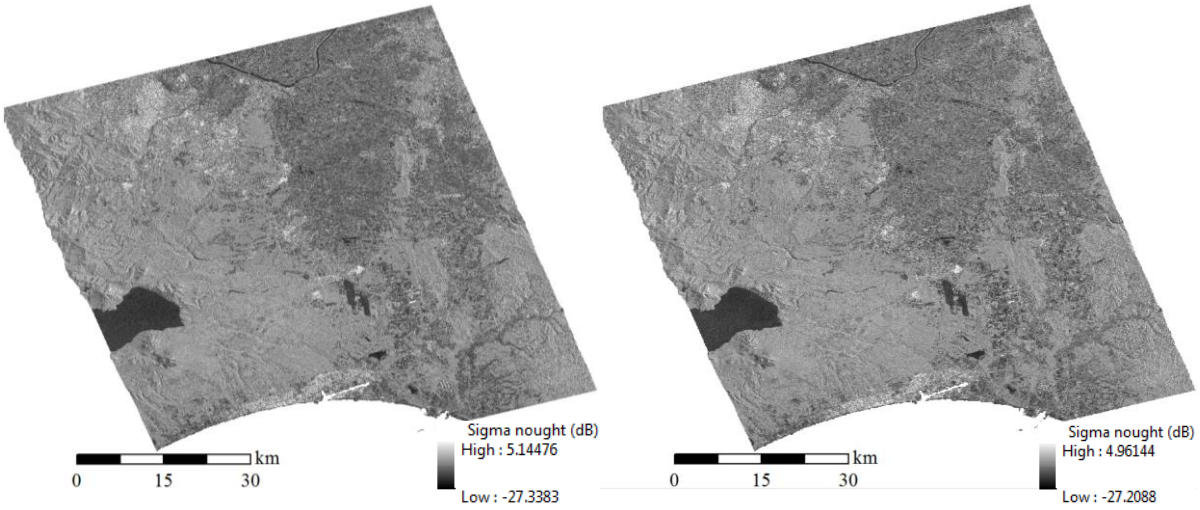

(a) Pre-event intensity image (b) Post-event intensity image

Figure 1. Pre- and post-event intensity images

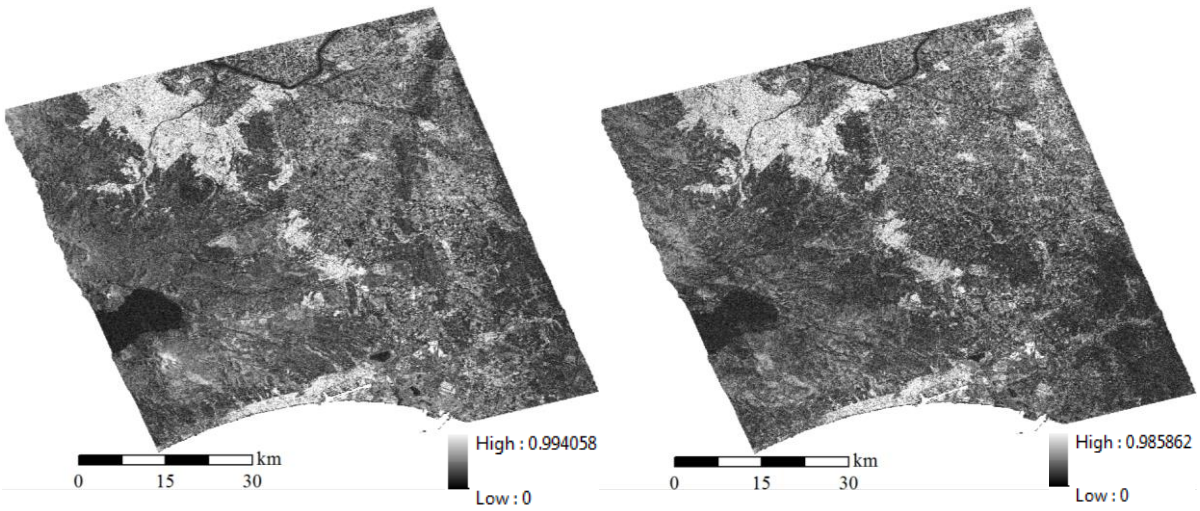

(a) Pre-event coherence image (b) Co-event coherence image

Figure 2. Pre- and co-event coherence images

After the basic intensity and coherence images were obtained, ArcGIS was applied to calculate the intensity difference image, the correlation coefficient image, and the normalized coherence difference image. The intensity difference and correlation coefficient images were calculated according to Eq. 1 and Eq.2, respectively. And the calculated images are shown in **Figure 3.** As the phase information is very sensitive to ground changes, instead of applying the co-coherence image directly, the normalized coherence image was calculated. The difference calculation of the pre- and co-coherence was to eliminate common changes in the two images caused by other effects. The normalization of the difference was executed to keep the data range between -1 and 1 (Eq.5) for easy and standard analysis. The final calculated normalized coherence difference image is shown in **Figure 4**.

$$\Delta\gamma = \frac{\gamma_{co} - \gamma_{pre}}{\gamma_{co} + \gamma_{pre}} \tag{5}$$

Where $\Delta\gamma$ means the normalized coherence difference, γ_{co} and γ_{pre} means the co- and pre-event coherence respectively.

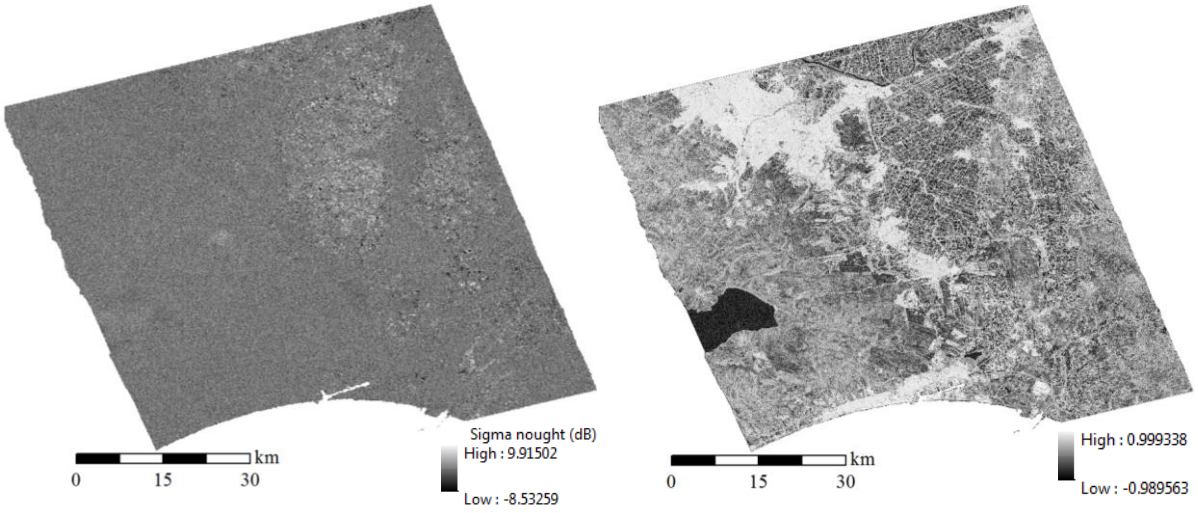

(a) Intensity difference image (b) Correlation coefficient image

Figure 3. Intensity difference and correlation coefficient images

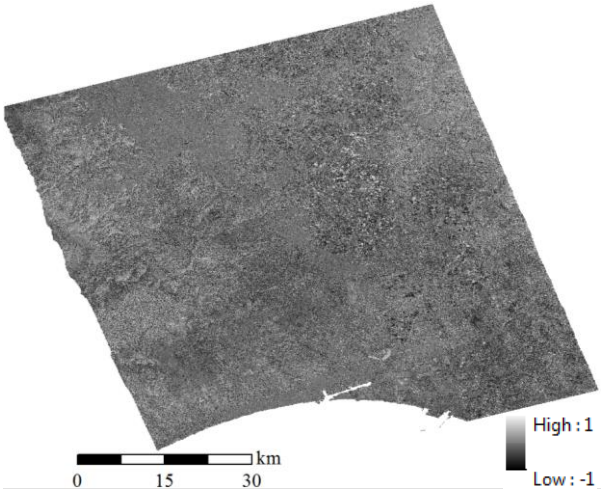

Figure 4. Normalized coherence difference image

Ground truth data making

To analyze the characteristics of the calculated parameters in the landslide areas, ground truth data are needed for delineating landslide extent and executing comparison. Google earth has published digital global imagery after the earthquake in the form of KML (2018). However, it cannot be converted into a layer in ArcGIS for direct application. Therefore the polygon tool in google earth was utilized to draw the triggered landslides within the SAR image boundary as shown in **Figure 5**. Then the drawn ground truth landslides were overlaid on the calculated parameter images in ArcGIS for easy interpretation and intuitive analysis.

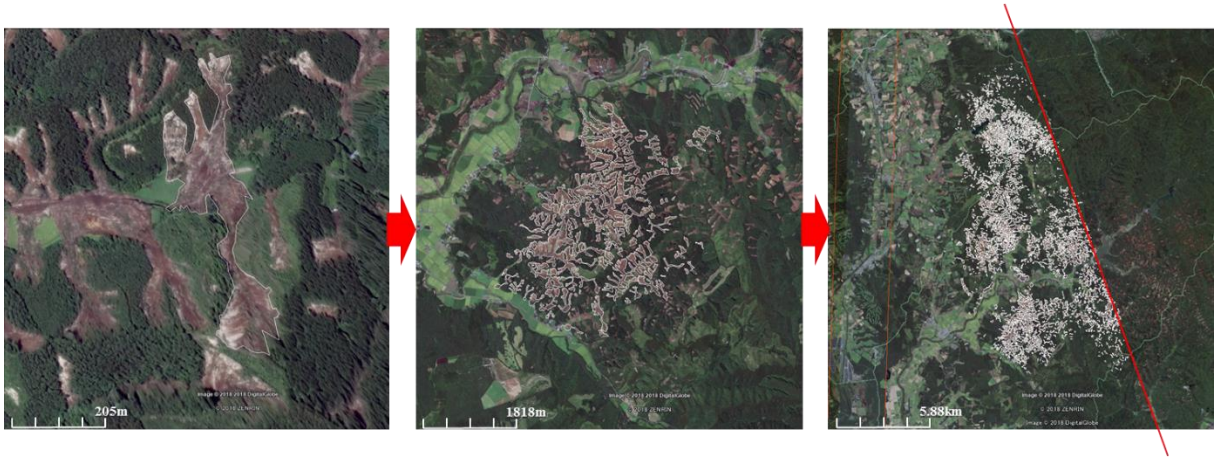

Figure 5. The process of drawing ground truth landslides (the polygons in the images indicate the drawn landslides, and the red line in the third image means the SAR image boundary)

Parameter analysis

After overlaying the drawn ground truth landslides on the calculated parameters, characteristics of these parameters in the landslide areas were analyzed separately to explore their capability in identifying landslides. In order to intuitively show the parameter characteristics in the landslide areas clearly, a small region in the entire map was taken out and shown in **Figure 6**.

As it can be seen from **Figure 6**, all of the three parameters show some differences in the landslide areas, and seems to have the capability for distinguishing landslide areas. In the intensity difference image (**Figure 6** (a)), the landslide areas show some obvious darker and brighter pixels.That means both increase and decrease of intensity have been caused by the earthquake-induced landslides. On one hand, landslides wiped away many stuffs on the hillside, such as trees, grass, big stones and soils, and smoothed the hillsides, leading to the reduction of backscattering from the ground to the radar sensor (i.e. the intensity decrease). On the other hand, the stuffs washed away by the landslides piled up in some area of the hill foot, increasing the backscattering of these areas and generating the bright pixels in the intensity difference image. Therefore, it seems that, from the intensity difference image, not only can the regions of landslides be seen, but also the direction of landslides can be roughly speculated, that is, from the darker pixel areas to the brighter pixel areas.

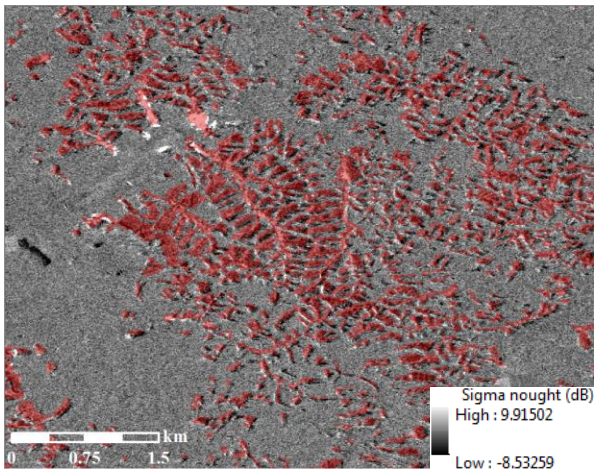

(a) Intensity difference

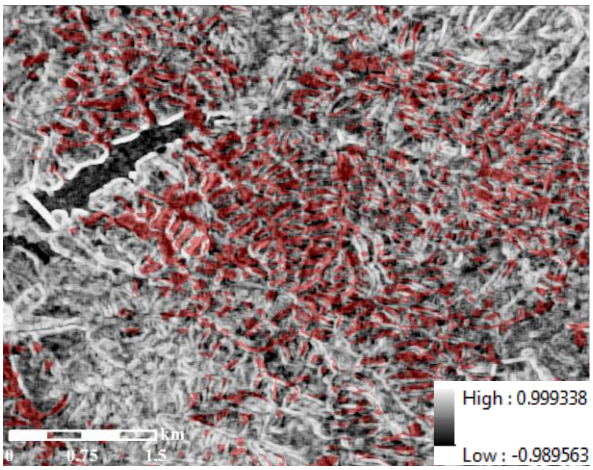

(b) Intensity correlation coefficient

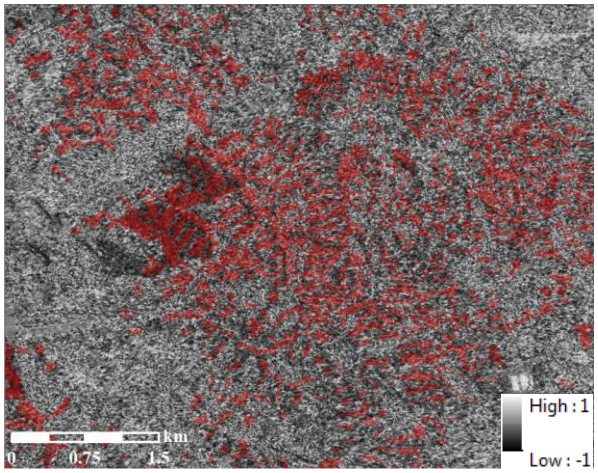

(c) Normalized coherence difference

Figure 6. Calculated parameters overlaid by ground truth landslides (the red polygons are the drawn ground truth landslides)

In addition, in the correlation coefficient image (**Figure 6** (b)), even though not very obvious, there are some darker pixels in the landslides and nearby regions. Due to the ground surface changes caused by the earthquake-induced landslides, the correlation coefficient value reduced, causing the darker pixels in the image. However, compared with the intensity difference image, the difference between the landslides and other areas seems to be obscure in the correlation coefficient image. Moreover, in the normalized coherence image (**Figure 6** (c)), the landslide areas also show darker pixels, meaning the coherence values decreased due to the earthquake-induced landslides. De-vegetation induced by landslides is considered as an importance reason for the de-coherence in the co-event coherence image, which caused the darker pixels in the normalized coherence difference image.

CONCLUSION

All of the intensity difference, correlation coefficient, and normalized coherence difference images show different characteristics in the earthquake-induced landslide areas, and seem to have the capability for the massive landslide mapping. The intensity difference image shows clear darker and brighter pixels in the earthquake-induced landslide areas, as triggered landslides smoothed the hillside areas and roughened the foothill areas. It can not only be used to detect the landslide regions, but also has the potential to roughly show the landslide direction. As the darker pixels were usually caused by the smoothing in the hillside areas, and brighter pixels were commonly induced by the piling up of alluvial deposits, the actual landslide direction can be inferred as the direction from the darker pixel areas to the brighter pixel areas. In addition, the normalized coherence difference image shows lower values in the landslide areas owing to the de-coherence in the co-event coherence image caused by landslide-induced ground changes, especially the de-vegetation. Moreover, the correlation coefficient image also shows lower values in the landslides and surrounding areas. However, compared with the intensity difference and normalized coherence difference images, the differences between the landslide areas and other regions are not very obvious in the correlation coefficient image. Further studies will focus on the quantitative comparison of the massive landslide mapping performance of the three parameters, and the relation construction between the actual landslides and the three potential parameters for future landslide mapping.

ACKNOWLEDGEMENT

ALOS-2 PALSAR-2 data is owned by the Japan Aerospace Exploration Agency (JAXA). This work has been undertaken within the framework of "Satellite image analysis support team for large scale disaster" of JAXA.

REFERENCES

Marano, K. D., Wald, D. J., & Allen, T. I. (2010). Global earthquake casualties due to secondary effects: a quantitative analysis for improving rapid loss analyses. Natural Hazards, 52(2), 319-328.

Cui, P., Zhu, Y. Y., Han, Y. S., Chen, X. Q., & Zhuang, J. Q. (2009). The 12 May Wenchuan earthquake-induced landslide lakes: distribution and preliminary risk evaluation. Landslides, 6(3), 209-223.

Strozzi, T., Farina, P., Corsini, A., Ambrosi, C., Manfred Thüring, & Zilger, J., et al. (2005). Survey and monitoring of landslide displacements by means of L-band satellite SAR interferometry. Landslides, 2(3), 193-201.

Confuorto, P., Di Martire, D., Centolanza, G., Iglesias, R., Mallorqui, J. J., & Novellino, A., et al. (2017). Post-failure evolution analysis of a rainfall-triggered landslide by multi-temporal interferometry SAR approaches integrated with geotechnical analysis. Remote Sensing of Environment, 188, 51-72.

Zhao, F., Mallorqui, J. J., Iglesias, R., Gili, J. A., & Corominas, J. (2018). Landslide monitoring using multi-temporal SAR interferometry with advanced persistent scatterers identification methods and super high-spatial resolution TerraSAR-X images. Remote Sensing, 10(6).

Mulas, M., Corsini, A., Cuozzo, G., Callegari, M., Thiebes, B., & Mair, V. (2016). Quantitative monitoring of surface movements on active landslides by multi-temporal, high resolution X-band SAR amplitude information: Preliminary results. 12th International Symposium on Landslides, Napoli, Italy, 1511–1516.

Xue, D., Yu, X., Jia, S., Chen, F., & Li, X. (2018). Study on landslide disaster extraction method based on spaceborne SAR remote sensing images – take ALOS PALSAR for an example. The International Archives of the Photogrammetry, Remote Sensing and Spatial Information Sciences, Beijing, China, XLII-3, 2023-2027.

Konishi, T., & Suga, Y. (2018). Landslide detection using COSMO-SkyMed images: a case study of a landslide event on Kii Peninsula, Japan. European Journal of Remote Sensing, 51(1), 205-221.

Burrows, K., Walters, R. J., Milledge, D., Spaans, K., & Densmore, A. L. (2019). A new method for large-scale landslide classification from satellite radar. Remote Sensing, 11(3).

M 6.6–27km E of Tomakomai, Japan. United States Geological Survey. Available online: https://earthquake.usgs.gov/earthquakes/eventpage/us2000h8ty/executive (last accessed on 7 March 2019).

Mainichi Shimbun. Damage from deadly Hokkaido quake estimated at over 367.5 billion yen. (2018). 4 October 2018. Retrieved 21 December 2018.

Yamagishi, H., & Yamazaki, F. (2018). Landslides by the 2018 Hokkaido Iburi-Tobu earthquake on September 6. Landslides, 15, 2521-2524.

JAXA. (2014) ALOS-2/PALSAR-2 Level 1.1/1.5/2.1/3.1 CEOS SAR Product Format Description.

ESA. Earthnet online. https://earth.esa.int/handbooks/asar/CNTR5-2.html (last accessed on 8 March 2019).

Massonnet, D., & Feigl, K. L. (1998). Radar interferometry and its application to changes in the earth's surface. Reviews of Geophysics, 36(4).

Zhao, C., Lu, Z., Zhang, Q., & Fuente, J. D. L. (2012). Large-area landslide detection and monitoring with ALOS/PALSAR imagery data over Northern California and Southern Oregon, USA. Remote Sensing of Environment, 124(9), 348–359.

Lanari, R., Fornaro, G., Riccio, D., Migliaccio, M., & Coltelli, M. (1996). Generation of digital elevation models by using SIR-C/X-SAR multifrequency two-pass interferometry: the Etna case study. IEEE Transactions on Geoscience and Remote Sensing, 34(5), 1097-1114.

Neelmeijer, J., Motagh, M., & Bookhagen, B. (2017). High-resolution digital elevation models from single-pass TanDEM-X interferometry over mountainous regions: a case study of Inylchek Glacier, Central Asia. ISPRS Journal of Photogrammetry and Remote Sensing, 130, 108-121.

Moreira, A., Prats-Iraola, P., Younis, M., Krieger, G., & Papathanassiou, K. P. (2013). A tutorial on synthetic aperture radar. IEEE Geoscience and Remote Sensing Magazine, 1(1), 6-43.

Veci, L. (2016). ALOS PALSAR orthorectification tutorial. ARRAY SYSTEM COMPUTING INC.

Karimzadeh, S., & Matsuoka, M. (2018). A weighted overlay method for liquefaction-related urban damage detection: a case study of the 6 September 2018 Hokkaido Eastern Iburi Earthquake, Japan. Geosciences, 8(12).

2018-hokkaido-earthquake-updated-imagery-nl. https://t.co/ncZBUbMkFj (last accessed on 8 March 2019).